

Publication VII

Tero Hottinen, Olli Himanen, "*PEMFC temperature distribution caused by inhomogeneous compression of GDL*", *Electrochemistry Communications* 9, pp. 1047-1052, 2007

© 2007 Elsevier Science

Reprinted with permission from Elsevier.

PEMFC temperature distribution caused by inhomogeneous compression of GDL

Tero Hottinen *, Olli Himanen

Helsinki University of Technology, Laboratory of Advanced Energy Systems, P.O. Box 2200, 02015 HUT, Finland

Received 2 November 2006; received in revised form 7 December 2006; accepted 8 December 2006

Available online 26 January 2007

Abstract

The effect of inhomogeneous compression of GDL under the channel/rib structure of flow-field plate on the temperature distribution in PEMFC is studied. The model utilizes experimentally evaluated GDL parameters for mass and charge transfer, and assumes an analogy between heat and charge transfer. The modeling results are compared with a conventional model that assumes the GDL properties constant. As a result, a significant difference in temperature distributions is observed especially due to varying thermal contact resistance at the GDL/electrode interface when the inhomogeneous compression is taken into account. There are significant temperature gradients through the cell and also in lateral direction of the electrode. With the assumed heat transfer parameters temperature differences of over 15 °C can be observed within a unit cell.

© 2006 Elsevier B.V. All rights reserved.

Keywords: PEMFC; Modeling; Temperature distribution; Gas diffusion layer; Inhomogeneous compression; Contact resistance

1. Introduction

One of the major obstacles for large-scale fuel cell commercialization is the reliability of the cells. Especially with polymer electrolyte membrane fuel cells (PEMFCs), possible hot-spots inside the cell enhance the degradation rate of the membrane causing lifetime limitations. One way to achieve more insight into the causes of these hot-spots, and hence enabling performance and lifetime optimization, is multiphysical modeling of the processes occurring inside the cell and its components.

One of the key components affecting the performance of a PEMFC is the gas diffusion layer (GDL). GDLs have to provide several functions for the fuel cell operation: a passage for reactant access and excess product water removal to and from the electrodes, electronic conductivity, heat removal, and adequate mechanical support for the mem-

brane electrode assembly (MEA). GDLs are typically made of highly porous carbon-fiber based paper or cloth in order to fulfill these requirements. High porosity gives a characteristic soft and brittle structure for the GDLs, which causes a deformation in its shape when the fuel cell is assembled and components compressed together.

The physical properties of GDL are changed under compression, and thus also its mass, heat, and charge transfer properties are changed. It has been experimentally shown that changes in the properties can have a significant effect on the fuel cell performance, see e.g. [1,2]. It is particularly worth noting that the deformation of GDL is not homogeneous. The parts of the GDL situated under the current collecting rib of the flow-field plate are significantly more compressed than the parts under the channel. This inhomogeneous compression causes significant changes in the local physical properties of GDL, and thus also in local species, current, and temperature profiles. The local changes of the mass and charge transfer parameters were studied experimentally by Nitta et al. [3]. It was observed that the GDL under the channel was practically not compressed causing significant changes in local properties.

* Corresponding author. Present address: Wärtsilä Corporation, Tekniikantie 14, 02150 Espoo, Finland. Tel.: +358 44 5838253; fax: +358 10 7099616.

E-mail address: tero.hottinen@wartsila.com (T. Hottinen).

The effect of inhomogeneous compression on the local cell performance was modeled by the author [4] with an isothermal model taking into account the experimentally evaluated parameters. It was observed that especially the variation in the contact resistance between electrode and GDL had a significant effect on the current distribution. The distribution was highly peaked because a notable portion of the current produced in the parts of the electrode situating under the channel flowed laterally in the electrode and entered the GDL at the point of lower contact resistance, i.e. under the rib.

It is believed that the observed changes in the current profile causes also significant changes in the temperature profile of the cell. The highly peaked current distribution causes a possible hot-spot because of Ohmic heating. In addition, because there is an analogy between heat and charge transfer, a notable portion of the heat generated in the electrode should also flow laterally before entering the GDL. This is possible only if there is a temperature gradient in the lateral direction of the electrode. This contribution is based on the model used in [4] with the inclusion of the energy equations and assuming an analogy between heat and charge transfer parameters. The non-isothermal modeling results are compared with a conventional model that excludes the effects on inhomogeneous compression.

2. Model

2.1. General

Two different cases are modeled: one with homogeneous properties of GDL (referred to as ‘base case’) and one where the inhomogeneous compression of GDL is taken into account. The used geometry is practically the same 2D cross-section of the cell used in [4], and the modeled geometries are illustrated in Fig. 1. The model consists of the anode and cathode GDLs and electrodes, and the membrane. The ribs and channels of the flow-field plates are

accounted for as boundary conditions. Only half-widths of the rib and channel structure and components below them are modeled, and the left and right geometry edges of Fig. 1 are modeled with symmetry boundary conditions, i.e. it is assumed that the cell geometry continues symmetrically to both directions.

The model takes into account the charge, heat, and multicomponent mass transfer in the cathode GDL and electrode, and charge and heat transfer in the membrane and anode GDL and electrode. The main assumptions of the model are that water exists only in gas phase and the anode activation and mass transfer limitations are negligibly small. The two-phase effects, with the exception that saturated water blocks the pores and thus reduces mass transfer rates, were excluded because there was no data available for capillary parameters as a function of compression. Thus the results of the model at the cell voltages lower than the voltage at which the liquid water saturation begins are only indicative. Even though the effects of inhomogeneous compression are taken into account also at the anode, the intrusion of the GDL into the channel is not included in the modeled geometry. This is made for simplicity, because the inclusion of it has an insignificantly small effect on the charge and heat transfer profiles of the anode GDL only.

2.2. Equations

Because the model that this contribution is based on is explained in details in [4], only the added energy equations and other modifications are described here. The used original equations are given in Table 1 with the fitted functions for the parameters affected by the inhomogeneous compression. A reliable estimate for contact resistance between GDL and electrode was not achieved in [3], and thus it is assumed to be the same as for GDL/current collector interface with a correction for Nafion content of the electrode (assumed to be 30 vol%). The boundary conditions are not repeated here, because they obey the normal Neumann

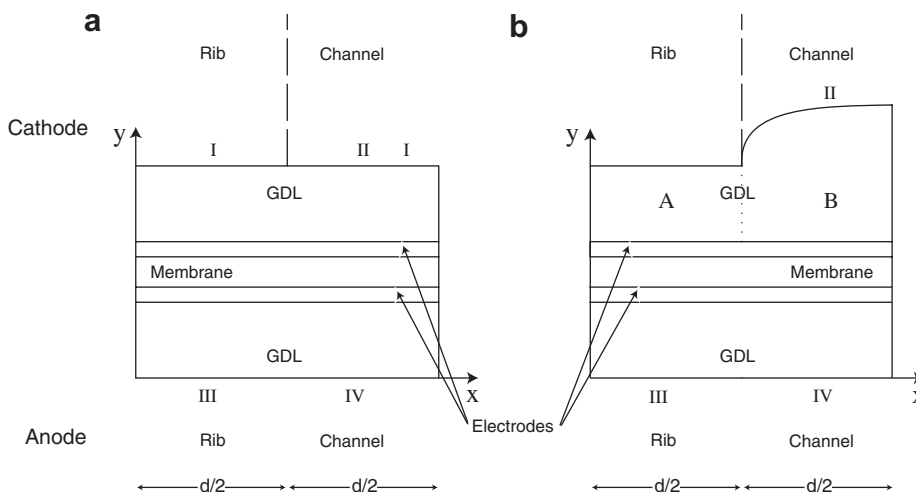


Fig. 1. Modeling domains: (a) geometry with homogeneous compression of GDL (base case); (b) geometry with inhomogeneous compression of GDL. The boundary domains are left out for clarity.

Table 1
Equations of the model used in [4]

Cathode GDL

$$\begin{aligned}\nabla \cdot (\rho \vec{v}) &= 0 \\ \nabla p &= -\frac{\mu}{k} \vec{v} \\ \nabla \cdot \vec{N}_i &= 0 \\ \nabla \cdot \left(-\sigma_{\text{GDL},x} \frac{\partial \phi_{\text{GDL},c}}{\partial x} \vec{e}_x - \sigma_{\text{GDL},y} \frac{\partial \phi_{\text{GDL},c}}{\partial y} \vec{e}_y \right) &= 0\end{aligned}$$

$$\begin{bmatrix} \vec{N}_{\text{O}_2} \\ \vec{N}_{\text{H}_2\text{O}} \end{bmatrix} = c \vec{v} \begin{bmatrix} X_{\text{O}_2} \\ X_{\text{H}_2\text{O}} \end{bmatrix} - c \bar{D}_{\text{eff}} \begin{bmatrix} \nabla X_{\text{O}_2} \\ \nabla X_{\text{H}_2\text{O}} \end{bmatrix}$$

$$c = \frac{p}{RT}$$

$$\rho = \frac{pM}{RT}$$

$$M = \sum_i X_i M_i$$

$$\bar{D}_{\text{eff}} = (\varepsilon(1-s))^{1.5} \bar{D}$$

$$s = \begin{cases} 0, & X_{\text{H}_2\text{O}} \leq \frac{p_{\text{sat}}}{p} \\ X_{\text{H}_2\text{O}} - \frac{p_{\text{sat}}}{p}, & X_{\text{H}_2\text{O}} > \frac{p_{\text{sat}}}{p} \end{cases}$$

$$\log_{10}(p_{\text{sat}}(\text{bar})) = 28.59051 - 8.2 \log(T + 0.01) + 0.0024804(T + 0.01) - \frac{3142.31}{(T+0.01)}$$

$$D_{11} = D_{\text{O}_2, \text{N}_2} (X_{\text{O}_2} D_{\text{H}_2\text{O}, \text{N}_2} + (1 - X_{\text{O}_2}) D_{\text{O}_2, \text{H}_2\text{O}}) / S$$

$$D_{12} = X_{\text{O}_2} D_{\text{H}_2\text{O}, \text{N}_2} (D_{\text{O}_2, \text{N}_2} - D_{\text{O}_2, \text{H}_2\text{O}}) / S$$

$$D_{11} = X_{\text{H}_2\text{O}} D_{\text{O}_2, \text{N}_2} (D_{\text{H}_2\text{O}, \text{N}_2} - D_{\text{O}_2, \text{H}_2\text{O}}) / S$$

$$D_{22} = D_{\text{H}_2\text{O}, \text{N}_2} (X_{\text{H}_2\text{O}} D_{\text{O}_2, \text{N}_2} + (1 - X_{\text{H}_2\text{O}}) D_{\text{O}_2, \text{H}_2\text{O}}) / S$$

$$S = X_{\text{O}_2} D_{\text{H}_2\text{O}, \text{N}_2} + X_{\text{H}_2\text{O}} D_{\text{O}_2, \text{N}_2} + X_{\text{N}_2} D_{\text{O}_2, \text{H}_2\text{O}}$$

$$D_{i,j} = \frac{p_0}{p} \left(\frac{T}{T_0} \right)^{1.5} D_{i,j}^0$$

$$X_{\text{N}_2} = 1 - X_{\text{H}_2\text{O}} - X_{\text{O}_2}$$

Cathode electrode

$$\nabla \cdot \vec{N}_{\text{O}_2} = -\frac{j_c}{4F}$$

$$\nabla \cdot \vec{N}_{\text{H}_2\text{O}} = \frac{j_c}{2F}$$

$$\nabla \cdot (-\sigma_e \nabla \phi_{e,c}) = j_c$$

$$\nabla \cdot (-\sigma_m \nabla \phi_m) = -j_c$$

$$j_c = j_{0,c} X_{\text{O}_2} \exp\left(\frac{-\alpha_e F}{RT} \eta\right)$$

$$\eta = \phi_{e,c} - \phi_m - E_0$$

Membrane

$$\nabla \cdot (-\sigma_m \nabla \phi_m) = 0$$

Anode electrode

$$\nabla \cdot (-\sigma_e \nabla \phi_{e,a}) = -j_a$$

$$\nabla \cdot (-\sigma_m \nabla \phi_m) = j_c$$

$$j_a = \frac{j_{0,a} \exp(\eta)}{RT} (\phi_{e,a} - \phi_m)$$

Anode GDL

$$\nabla \cdot \left(-\sigma_{\text{GDL},x} \frac{\partial \phi_{\text{GDL},a}}{\partial x} \vec{e}_x - \sigma_{\text{GDL},y} \frac{\partial \phi_{\text{GDL},a}}{\partial y} \vec{e}_y \right) = 0$$

Effect of inhomogeneous compression

$$h(x) = \begin{cases} h_{\text{comp}}, & x \in A \\ 19.30314 \ln((x - 0.0005) * 10^6 + 1) * 10^{-6} + h_{\text{comp}}, & x \in B \end{cases} \quad [\text{m}]$$

$$\varepsilon(x) = \varepsilon_0 \frac{h(x) - h_{\text{min}}}{h_0 - h_{\text{min}}}$$

$$h_{\text{min}} = (1 - \varepsilon_0) h_0$$

$$k(x) = -1.700 * 10^{-11} + 2.760 * 10^{-7} h(x) - 1.484 * 10^{-3} h(x)^2$$

$$+ 2.754 h(x)^3 \quad [\text{m}^2]$$

$$\sigma_{\text{GDL},x}(x) = 6896 - 1.159 * 10^7 h(x) \quad [\Omega^{-1} \text{m}^{-1}]$$

$$\sigma_{\text{GDL},y}(x) = 3285 - 8.385 * 10^6 h(x) \quad [\Omega^{-1} \text{m}^{-1}]$$

$$r_{\text{cont},\text{gr}}(x) = 5.83 * 10^{-10} \exp(2.06 * 10^4 h(x)) \quad [\Omega \text{m}^2]$$

$$r_{\text{cont},e}(x) = \frac{1}{1-0.3} r_{\text{cont},\text{gr}}(x) = 1.429 r_{\text{cont},\text{gr}}(x) \quad [\Omega \text{m}^2]$$

and Dirichlet –type conditions, and can be found in most of the fuel cell modeling papers.

When the contact resistances are taken into account with heat transfer, there is a discontinuity in temperature

because of thermal contact resistance and discontinuity in heat flux due to Ohmic heating resulting from electric contact resistance. It was impossible to take both of these thermal effects into account as a boundary condition, and thus the contact resistance effects were taken into account by modeling the boundary as a thin layer of its own. The electric and heat conductivities of the boundary layer were calculated so that its total heat and charge transfer resistances corresponded to the used contact resistance values. The mass transfer properties of the boundary layer were taken to be similar to GDL. It was observed that approximating the contacts with a 0.5 μm thick boundary layer causes less than 0.1% difference in average current densities and less than 1% difference in local values compared to the results achieved in [4].

The heat in the fuel cell components is transferred by conduction and convection. The mass transfer was neglected at the anode and membrane, and thus there is only conduction present at those components. The conductive and convective heat fluxes can be calculated as

$$\dot{q}_{\text{cond}} = - \left(\kappa_x \frac{\partial T}{\partial x} \vec{e}_x + \kappa_y \frac{\partial T}{\partial y} \vec{e}_y \right) \quad (1)$$

$$\dot{q}_{\text{conv}} = \sum_i \vec{N}_i M_i C_{p,i} T \quad (2)$$

The governing equation for heat transfer is

$$\nabla \cdot \dot{q} = \sum_i P_i \quad (3)$$

where different heat source terms are due to Ohmic heating, irreversible potential losses due to reactions, and entropy production, and can be described as

$$P_{\text{ohmic}} = \sigma (\nabla \phi)^2 \quad (4)$$

$$P_{\text{irr}} = -j \eta \quad (5)$$

$$P_{\text{entr}} = \frac{-j T \Delta S}{z F} \quad (6)$$

Ohmic heating is present in all of the components, and the other source terms are present only at the electrodes where the reactions occur. It is assumed that the entropy production caused by the reactions is directly changed into sensible heat at the point of electrode where the corresponding reaction occurs.

The temperature dependency of exchange current density was taken from [5]:

$$j_{0,c}(T) = j_{0,c}(T_0) \exp\left(\frac{-\Delta E_{\text{exc}}}{R} (T^{-1} - T_0^{-1})\right) \quad (7)$$

The temperature dependency of the anode exchange current density was not taken into account due to lack of data and because its effect is insignificant due to fast anode kinetics.

It is assumed that the cooling system is efficient enough to keep the current collector in constant temperature, and that all of the heat is removed through it. This yields boundary conditions for boundaries I and III:

Table 2
Dimensions of the modeled geometries

| Parameter | Symbol | Value |
|----------------------------|-------------------|-------------------|
| Channel and rib width | d | 1 mm |
| Uncompressed GDL thickness | h_0 | 380 μm |
| Compressed GDL thickness | h_{comp} | 250 μm |
| Electrode thickness | | 10 μm |
| Membrane thickness | | 25 μm |
| Boundary layer thickness | | 0.5 μm |

$$T = T_0 \quad (8)$$

and for boundaries II and IV:

$$\frac{\partial T}{\partial y} \vec{e}_y = 0 \quad (9)$$

2.3. Parameters and model solving

The dimensions of the modeled geometries are given in Table 2. The constants and parameters used in the model are listed in Table 3. Standard textbook values for constants and typical values found in the PEMFC modeling articles for fuel cell parameters are used when a reference is not given. All of the electrode parameters are assumed as bulk constants due to lack of reliable measured data, even though the inhomogeneous compression of GDL most probably affects these too.

The heat transfer parameters are calculated assuming that the analogy between heat and charge transfer holds.

Table 3
Constants and parameter values

| Parameter | Symbol | Value |
|--|--|--|
| Activation energy | E_{exc} | 76.5 kJ mol ⁻¹ , $E_{\text{cell}} \geq 0.8$ V [5], 27.7 kJ mol ⁻¹ , $E_{\text{cell}} < 0.8$ V [5] |
| Ambient pressure | p_0 | 101325 Pa |
| Binary diffusion coefficient O ₂ , H ₂ O | $D_{\text{O}_2, \text{H}_2\text{O}}^0$ | 3.98 * 10 ⁻⁵ m ² s ⁻¹ |
| Binary diffusion coefficient O ₂ , N ₂ | $D_{\text{O}_2, \text{N}_2}^0$ | 2.95 * 10 ⁻⁵ m ² s ⁻¹ |
| Binary diffusion coefficient H ₂ O, N ₂ | $D_{\text{H}_2\text{O}, \text{N}_2}^0$ | 4.16 * 10 ⁻⁵ m ² s ⁻¹ |
| Conductivity of electrode | σ_e | 300 Ω^{-1} m ⁻¹ [3] |
| Entropy production, cathode | ΔS_c | -326.36 J mol ⁻¹ K ⁻¹ [7] |
| Entropy production, anode | ΔS_a | 0.104 J mol ⁻¹ K ⁻¹ [7] |
| Exchange current density, cathode | $j_{0,c}$ | 20 * 10 ³ A m ⁻³ |
| Exchange current density, anode | $j_{0,a}$ | 1.7 * 10 ⁹ A m ⁻³ |
| Faraday constant | F | 96487 As mol ⁻¹ |
| Gas constant | R | 8.314 J mol ⁻¹ K ⁻¹ |
| Heat capacity of oxygen | C_{p, O_2} | 923 J kg ⁻¹ K ⁻¹ |
| Heat capacity of water | $C_{p, \text{H}_2\text{O}}$ | 1996 J kg ⁻¹ K ⁻¹ |
| Heat conductivity of electrode | κ_e | 0.1 W m ⁻¹ K ⁻¹ |
| Heat conductivity of membrane | κ_m | 0.05 W m ⁻¹ K ⁻¹ |
| Molar mass of oxygen | M_{O_2} | 0.032 kg mol ⁻¹ |
| Molar mass of water | $M_{\text{H}_2\text{O}}$ | 0.018 kg mol ⁻¹ |
| Molar mass of nitrogen | M_{N_2} | 0.028 kg mol ⁻¹ |
| Permeability of electrode | k_e | 1.26 * 10 ⁻¹³ m ² [8] |
| Porosity of uncompressed GDL | ε_0 | 0.84 [9] |
| Porosity of electrode | ε_e | 0.4 |
| Protonic conductivity | σ_m | 5 Ω^{-1} m ⁻¹ |
| Reaction symmetry factor | α_r | 0.5 |
| Reversible cell potential | E_0 | 1.23 V |
| Temperature | T_0 | 323.15 K |
| Viscosity of air | μ | 1.9 * 10 ⁻⁵ kg m ⁻¹ s ⁻¹ |

The reference values for the analogy are taken to be the electrode heat conductivity based on the results and discussion in [6] and the electrode electric conductivity measured in [3]. It has to be pointed out that even though the analogy between heat and charge transfer is typically valid for most conditions and materials, this is not necessarily the case with electrode where there is besides heat and charge transfer also chemical energy converted into heat and work. However, due to lack of reliable measured parameters, the analogy is assumed valid here. The heat conductivities for boundary layers and GDL are calculated via relation:

$$\kappa_i = \frac{\kappa_e}{\sigma_e} \sigma_i \quad (10)$$

The modeling was done using a commercial finite element method program COMSOL Multiphysics version 3.2b with a parametric nonlinear direct solver. When solving the model, the cell voltage was used as a fixed parameter by setting the potential of anode current collector to zero and the potential of cathode current collector to cell voltage. The used degrees of freedom were 236,484 for base case and 232,394 for the inhomogeneous compression.

3. Results

The polarization curves of different simulated cases are illustrated in Fig. 2. The average cell performance is only slightly decreased when the inhomogeneous compression is taken into account. The liquid water saturation with dif-

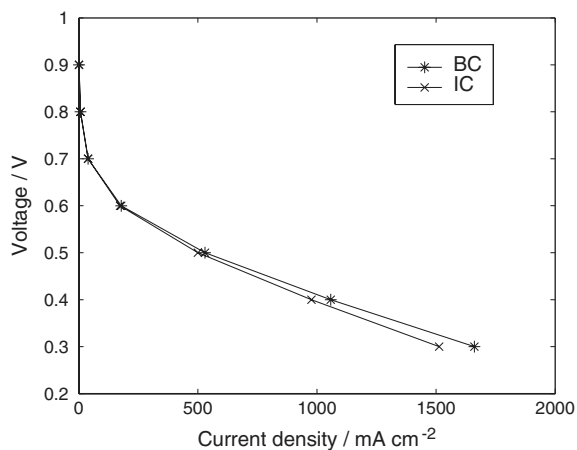


Fig. 2. Polarization curves. ‘BC’ refers to the base case and ‘IC’ to inhomogeneous compression.

ferent simulated cases begins at 0.485–0.501 V, and thus the results below 0.5 V are not discussed here.

The current production rates at the cathode electrode at 0.5 V are illustrated in Fig. 3. The current production rates for the base case increase from the middle of the rib to the middle of the channel due to higher oxygen concentration. When the inhomogeneous compression is taken into account, there is a significant difference in the current production rates. The rates increase from the middle of the channel to the edge of the channel due to higher oxygen concentration, but are drastically decreased under the

channel. This is caused by the higher resistive losses due to significantly higher contact resistance. Increased temperature also decreases the exponential term in the Butler–Volmer equation in Table 1 causing decreased current production rate, but this is practically compensated by the increased exchange current density.

Temperature profiles from the upper boundary of the electrode and from the middle plane of the boundary layer are illustrated in Fig. 4. With constant GDL properties there is only a smooth increase in temperature due to higher reaction rates under the channel than under the current collecting rib. The temperature profile shapes are very similar at both planes. The temperature difference across the boundary layer, i.e. the jump caused by thermal contact resistance, is approximately 1.2 °C. The difference between the maximum and minimum temperatures of the whole cell is approximately 4.9 °C.

When the inhomogeneous compression is taken into account, the thermal contact resistance causes a significant change in the temperature profiles under the channel even though the reaction rates are smaller. A notable portion of the heat produced under the channel is conducted in lateral direction in the electrode and enters the GDL under the rib, where there is a smaller thermal contact resistance, causing a significant temperature gradient inside the electrode. A similar result was achieved for charge transfer in [4], where there was a notable lateral current inside the electrode observed. The temperature differences across the boundary layer vary approximately from 1.2 °C to

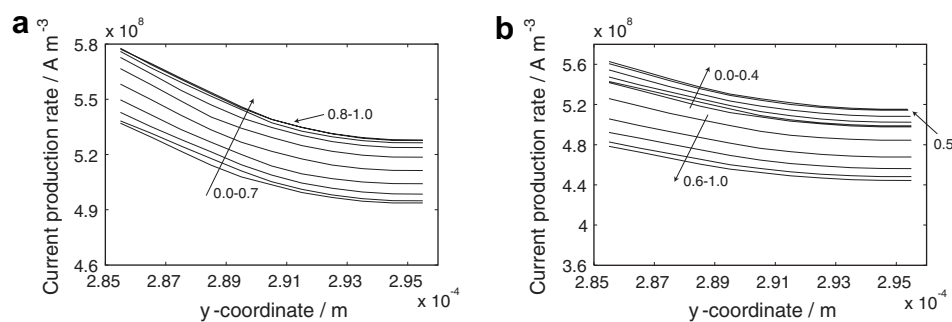


Fig. 3. Current production profiles at the cathode electrode: (a) for the base case (b) for the inhomogeneous compression. The profiles are current production rates in y -direction drawn at every 0.1 mm in x -direction. The arrows show the direction of increasing x -axis and labels the corresponding values in millimeters.

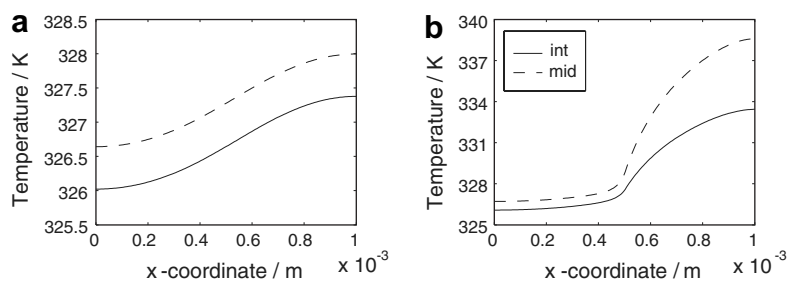


Fig. 4. Temperature profiles at the interface between electrode and boundary layer (‘int’), and in the middle of the boundary layer (‘mid’) at 0.5 V: (a) base case; (b) inhomogeneous compression.

10.3 °C. The difference between the maximum and minimum temperatures of the whole cell was approximately 15.5 °C.

4. Summary and discussion

This paper focused on modeling the thermal effects that the inhomogeneous compression of PEMFC gas diffusion layer has. Model took into account the multicomponent mass transfer in the cathode components, and charge and heat transfer in all of the cell components. The model was based on the non-isothermal one-phase model presented in [4] with the inclusion of energy equations. The experimental parameters evaluated in [3] were used for mass and charge transfer, and an analogy between heat and charge transfer parameters was assumed.

The reaction rates below the channel parts of the electrode were significantly changed when the inhomogeneous compression was taken into account. The reason was that the losses were increased by the higher electric contact resistance. The reaction rates were also reduced due to higher temperature because of the decrease in the exponential term in the Butler–Volmer equation but this reduction was compensated by the increased exchange current density.

Also the temperature profiles were significantly changed due to inhomogeneous compression. A notable portion of the heat generated in the electrode under the channel flowed laterally and entered the GDL under the rib where there was lower thermal contact resistance. This caused a significant temperature gradient within the electrode and the whole cell.

The observed temperature differences within the cell can have tremendous effects for practical cell design. The places with higher temperature are more prone to degradation causing possible lifetime problems, and thus the temperature distribution should be as homogeneous as possible. One possible way to accomplish this is minimizing the parts of the GDL having low compression pressure with narrower channels. However, narrowing the channels has its limitations due to manufacturing cost and tolerances. In addition, the pressure drop increases when the channel dimensions are decreased causing limitations of its own.

The effect of rib structure has also to be taken into account in order not to interfere the mass transfer below the ribs. Besides affecting the design of the channel/rib structure, the inhomogeneous compression also affects the design of flow pattern between anode and cathode. In order to minimize areas having low heat transfer properties at both sides of the cell, the main channel direction should be in the cross-flow mode.

Even though the results imply that there exists a more significant temperature difference inside a PEMFC than a model excluding the inhomogeneous compression of GDL would predict, it has to be pointed out that the parameters used for the simulation were based on assumptions and the model was in one phase. Thus, the detailed analysis of temperature and liquid water distributions requires the heat and capillary mass transfer parameters to be measured as a function of GDL thickness as was done in [3] for mass and charge transfer parameters.

Acknowledgement

The financial support of the Academy of Finland (decision 206132) is gratefully acknowledged.

References

- [1] W.-K. Lee, C.-H. Ho, J.W. Van Zee, M. Murthy, *J. Power Sources* 84 (1999) 45–51.
- [2] J. Ge, A. Higier, H. Liu, Effect of gas diffusion layer compression on PEM fuel cell performance, *J. Power Sources* 159 (2006) 922–927.
- [3] I. Nitta, T. Hottinen, O. Himanen, M. Mikkola, Inhomogeneous compression of PEMFC gas diffusion layer – Part I: Experimental, *J. Power Sources*, in press.
- [4] T. Hottinen, O. Himanen, S. Karvonen, I. Nitta, Inhomogeneous compression of PEMFC gas diffusion layer – Part I: Modeling the effect, *J. Power Sources*, in press.
- [5] W. Sun, B.A. Peppley, K. Karan, *Electrochim. Acta* 50 (2005) 3359–3374.
- [6] P.J.S. Vie, S. Kjelstrup, *Electrochim. Acta* 49 (2004) 1069–1077.
- [7] M.J. Lampinen, M. Fomino, *J. Electrochem. Soc.* 140 (1993) 3537–3546.
- [8] O. Himanen, T. Hottinen, M. Mikkola, V. Saarinen, *Electrochim. Acta* 52 (2006) 206–214.
- [9] Manufacturer's data sheet for [®]Sigracet GDL 10 BA by SGL Carbon AG.